Drop Testing Campaign and Simulation Results for a Magnetic Bearing Supported Blower for Space Applications

Larry Hawkins*, Scott Tran*, Nick Fruth*, Rasish Khatri*, and Chris Brown**
*Calnetix Technologies, Cypress, CA, USA
E-mail: lhawkins@calnetix.com
**NASA International Space Station Vehicle Office, Houston, TX, USA

Abstract
NASA developed and has deployed aboard the International Space Station (ISS) a next-generation CO2 removal system, the Four Bed Carbon Dioxide Scrubber (4BCO2) for use as a testbed. A key component of both the existing and the new system is the blower that provides the airflow through the CO2 sorbent beds. To improve performance and reliability, magnetic bearings are used instead of more conventional bearings (e.g. ball bearings or air bearings). The new blower, described in [1], features a high-efficiency permanent magnet motor, a five-axis, active magnetic bearing system, backup bearing system, and a compact controller containing both a variable speed drive and magnetic bearing controller. The blower, commissioned aboard the ISS in February 2023, recently passed two years of operation. Due to the remoteness of the ISS and potential for use of the new blower in future missions, NASA recently funded a drop testing program to validate life of the backup bearings out to 100 drops and spin downs from operating speed. The test program is described here, trend data and high-fidelity position sensor data are presented and described, and post-test hardware photos are discussed. Simulation results are also presented and compared to the measured data.

Keywords : Backup bearings, Touchdown bearings, drop or landing tests

1. Introduction

A blower supported by active magnetic bearings (AMBs) has been operating on the ISS as part of a CO2 scrubber (4BCO2) since February 2023. The blower, shown in Figure 1, includes a centrifugal impeller driven by a permanent magnet synchronous motor (PMSM), a five-axis, active magnetic bearing system, and a compact controller containing both a variable speed drive and magnetic bearing controller. Design of the blower system AMBs, the backup bearings, and preliminary rotor drop simulations were discussed by Hawkins [1]. Launch vibration simulation and testing, and operation data from the ISS have also been discussed in the literature [2,3]. The design is briefly reviewed here to provide background to the reader.

The blower, commissioned aboard the ISS in February 2023, recently passed two years of operation. Due to the remoteness of the ISS and potential for use of the new blower in future missions, NASA recently funded a drop testing program to validate life of the backup bearings out to 100 drops and spin downs from operating speed. The test program is described here, trend data and high-fidelity position sensor data are presented and described, and post-test hardware photos are discussed. Simulation results are also presented and compared to the measured data.

The target of 100 drops and spin downs, which is considerably higher than the typical 5 to 10 drop/spin down requirement for an industrial machine, was set to account for potential power loss events over the course of the remaining ISS life. This extended life is possible because of several characteristics of the blower:

1) The max spin speed is relatively low (60,000 rpm) for a rotor of this small size, such that there is substantial rotordynamic margin to the first bending mode frequency. This allows a robust backup bearing design (low max Hertzian contact stress) with low speed factor (*ndm*<1e6 mm-rpm at max speed).
2) The aerodynamic drag from the impeller after shut down brings the rotor from 60,000 rpm to rest in 10-12 seconds.
3) The ambient temperature is low (~20C above cabin air temperature).

2. Blower Configuration

Detail design of the blower, magnetic bearings and backup bearings has been previously reported [1]. The design is briefly described here for reference. Figure 1 shows the overall layout of the blower. The centrifugal impeller at the inlet (right side) draws in cabin air and pushes it through an annular passage to the outlet. The drive motor near the outlet (left side) is cooled by a bypass flow. The blower is designed to be operated at any speed from rest up to 60,000 rpm.

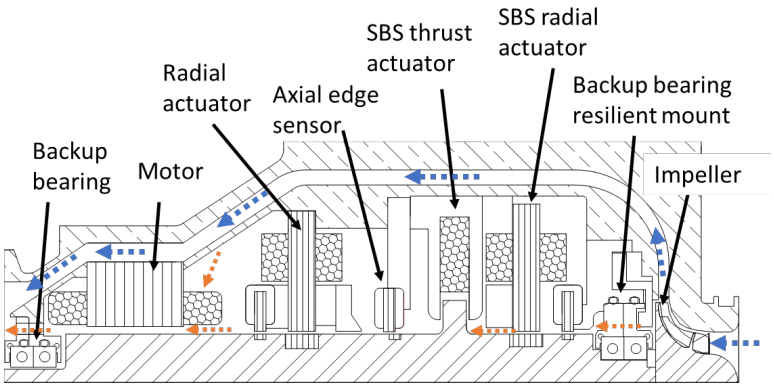

Fig 1. Layout of blower for the new 4BCO2 system (from Fig. 2 of [1]).

Table1. Magnetic Bearing Design Parameters

Parameter	Radial Brg1	Radial Brg2	Axial
Load capacity N (lbf)	44 (10)	44 (10)	89 (20)
Force constant N/A (lbf/A)	18.5 (4.2)	18.5 (4.2)	38.3 (8.61)
Neg. stiffness N/mm (lbf/in)	173 (990)	89 (510)	70 (400)

The homopolar, permanent magnet (PM) biased magnetic bearings are centrally located. A two-axis radial active magnetic bearing is adjacent to the motor and a three-axis combination radial/thrust active magnetic bearing is at the impeller end. The basic design parameters for the magnetic bearings are summarized in Table 1. The radial position sensors are located just outboard of the actuators and the axial position sensor is between the two magnetic bearing sets. The backup bearings are comprised of resiliently mounted, angular contact ball bearings. The backup bearings serve to support the shaft when the magnetic bearings are de-activated, in the case of overload, or in the case of a critical component failure. The first forward free/free bending mode of the rotor is 2.3 kHz at 0 rpm and 2.4 kHz at 60,000. The rotor mass is 0.70 kg (1.53 lbm).

3. Backup Bearing Configuration

The impeller end (inlet), radial/thrust (combination) backup bearing assembly is shown in Fig. 2. Selected dynamic characteristics for the bearings and mount are given in Table 2. The motor end (outlet), radial only, backup bearing assembly uses smaller bearings and does not include rotor mounted thrust surfaces but is otherwise similar. The bearings are angular contact, duplex pairs with a full complement (no cage) of ceramic balls. The bearings are unlubricated due to previous dust contamination issues with the legacy foil bearing blower; however, the bearing rings are silver plated to add lubricity. Each backup bearing pair is supported in a resilient mount where elastomeric O-rings are used to lower effective stiffness and provide damping. These characteristics limit peak impact loads during the rotor drop transient, add damping, and lower the rigid body natural frequencies. Lowering the rigid body natural frequencies lowers the frequency of forward whirl that occurs during drop and spin down with axial load and low or no radial load [4].

Although, effective and suitable for backup bearing mount applications, the designer must recognize that elastomers become stiffer as frequency increases and softer as temperature increases. Additionally, with the stiffness of O-rings increases with pre-strain (squeeze) as this increases the effective area/thickness ratio [5].

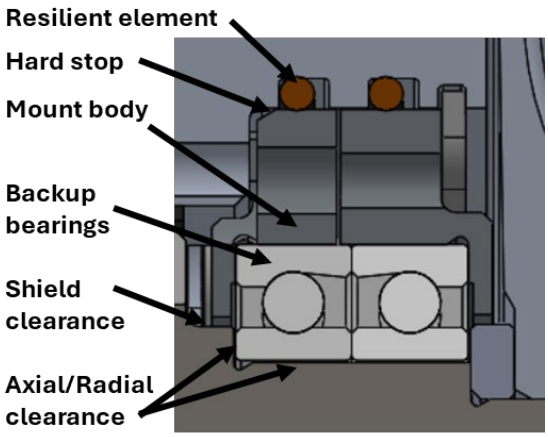

Fig. 2. Inlet end (radial/thrust) backup bearing assembly.

Table2. Backup Bearing and Mount Characteristics

Parameter	Radial Brg1	Radial Brg2	Axial
Free Clearance mm (in)	0.152 (0.006)	0.127 (0.0045)	0.127 (0.005)
Resilient Mnt Travel mm (in)	0.076 (0.003)	0.076 (0.003)	0.051 (0.002)
Backup Bearing Stiff (pair), N/mm (lbf/in)	22,800 (130,000)	43,800 (250,000)	9,600 (55,000)
Resilient Mnt Stiff N/mm (lbf/mil)	450/900 (2.6/5.2)	550/1,100 (3.0/6.0)	--
Radial Hard Stop Stiffness N/mm (lbf/in)	114,000 (650,000)	220,000 (1,250,000)	48,000 (275,000)

The speed factors, *ndm*, of the backup bearings are 0.81E6 and 1.08E6 mm-rpm at 60,000 rpm, where *n* is the speed in rpm and dm is the average of the inside and outside diameter. The speed factors are lower than usual for backup bearings, a design feature made possible due to the relatively low maximum spin speed for a rotor of this size. The combination of low speed factor, high load margin and low temperature environment (40°C - 60°C), is expected to lead to a survivability of >100 drop spin down cycles with minimal wear.

4. Test Program and Results

An Engineering Development Unit (EDU) blower was used for the testing. The EDU is identical to the flight unit installed on the ISS. As it is not practical to replicate the micro gravity conditions of the ISS, rotor drop testing was performed using two spin axis orientations (horizontal and vertical) as a suitable compromise. Compared to potential unplanned drop/spin downs in space, horizontal drop testing on earth is slightly less severe and vertical drop testing on earth is slightly more severe. With gravity and horizontal orientation, the gravity load is 3.1 N (0.70 lbf) and 3.7 N (0.83 lbf) at Radial Brg1 and Radial Brg2 respectively. Caprio [6] showed that a fixed direction static radial load can suppress forward whirl, so the total load during spin down should be reduced. With gravity and vertical orientation, the axial load is higher by 6.8 N (1.53 lbf). The extra axial gravity load for vertical testing is expected to increase the forward tangential force at the axial bearing contact [4], likely increasing the forward whirl frequency and/or whirl duration when compared to space. Regardless of the existence of gravity, there is an aerodynamic thrust of 13.3N (3.0 lbf) at full speed that declines with speed squared. There are also negative stiffness loads from the PM bias magnetic bearings that pull the rotor against the backup bearings when the control is de-energized, regardless of the existence of gravity. These increase the overall bearing loads, but also reduce bouncing, particularly useful in microgravity.

Two sets of new backup bearings were tested per the schedule given in Table 3. The first set was tested to 30 drop/spin down events from 60,000 rpm to rest; the bearings were then inspected by an outside vendor and shown to have minimal wear. The second set was tested to 100 drop/spin downs and inspected by an outside vendor after 60 drops and 100 drops. High sample rate rotor displacement signals from the AMB sensors were monitored and stored for each drop event along with outer ring temperature measurements.

Table 3. Drop Test Schedule

Bearing set	Drop number	Orientation	Notes
#1	1-5, 11-20	Horizontal	• Inspection of bearings and rotor surface at CNX after drop 10 and 20 • Bearings inspected by outside vendor after drop 30
	6-10, 21-30	Vertical	
#2	1-10, 21-30 41-50, 61-70, 81-90	Horizontal	• Inspection of bearings and rotor surface at CNX after drop 20 and 40 • Bearings inspected by outside vendor after drop 60 • Bearings inspection by outside vendor after drop 100
	11-20, 31-40 51-60, 71-80, 91-100	Vertical	
Drop speed is 60,000 rpm for all tests.			

4.1 Test Procedure

The drop testing was conducted using the following steps:

1) Spin blower to 60kRPM set blower delta pressure to ISS operating point (46.5in-H2O @ ~30SCFM).
2) Dwell until bearing temperature is stable (varies less than 0.2°C / minute). The steady temperatures of the bearing outer rings were typically 43 °C at the inlet (Brg2) and 48 °C at the outlet bearing (Brg1).
3) Activate test mode to allow delevitation at speed; wait 10 sec, then de-levitate rotor.
4) MBC detects contact fault condition (0.75 sec filtered delay) and trips motor.
5) Wait for the rotor to coast to a stop, then take screenshots of the GUI main screen.
6) Wait 5 minutes post drop, then reset faults, levitate rotor, and take a screenshot of the GUI main screen.
7) Run a levitated 5-axis clearance check measurement.
8) Delevitate rotor and use the MBC GUI to command a 2.5A circular current at 1Hz while recording data.
9) Position sensor data recorded at 5 kHz, temperature and synchronous data recorded at 1 Hz during testing.
10) Review data and repeat starting from step 1 for the next drop (~ 1 hour delay minimum).

4.2 Test Results

Figures 3-6 show displacement data from the thrust end (Brg2) position sensors for drop 60 (vertical). Figure 3a shows an overall time history of the drop, and Figure 3b shows a zoom around the initial drop, contact and establishment of whirl. The initial contact is made at 11.373 sec, followed by a few bounces of the rotor. The rotor then executes two backward whirl orbits as the backup bearing inner ring and ball train come up to speed. Note that the forward spin direction is *y* leading *x* on this machine. At about 11.44 seconds the rotor reverses and enters forward whirl. At about 12.1 sec (0.75 sec post drop), the MBC contact fault trips the motor and the rotor coasts to rest driven primarily by the pumping losses of the compressor.

Figure 4 shows orbit plots measured from the *x/y* position sensors. Figure 4a is for the first 0.08 sec of the drop – up to the point where the rotor reverses to forward whirl. Figure 4b shows the orbit as the rotor speed declines from 57 krpm to 50 krpm during the spin down. The orbit radius at the position sensors is approximately 150 um (5.9 mil) with a whirl frequency of ~175 Hz. The whirl frequency depends primarily on the lowest rotor rigid body mode frequency, the axial force reacted by the thrust backup bearing, and coefficient of friction at the axial bearing rotor contact surface. Figure 4c shows the orbit as the rotor speed declines from 20 krpm to 15 krpm during the spin down. The orbit radius is lower at ~130 um (5.1 mil) with a whirl frequency of ~150 Hz. Now the whirl orbit tends to not execute a full circle around the bearing bore. The observed behavior and orbit size compares well with the simulation results presented below.

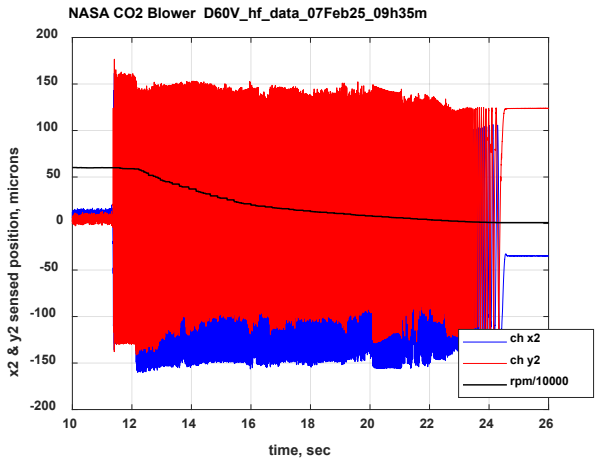

Figure 3a. Position vs. time for x2 and y2 sensors, during drop and spin down, vertical rotor, drop 60.

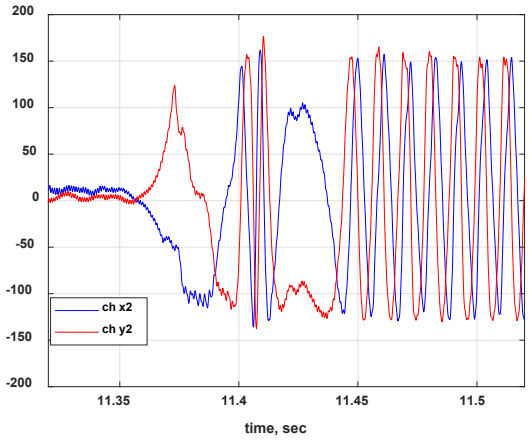

Figure 3b. Position vs. time for x2 and y2 sensors, during initial portion of drop 60 with vertical rotor.

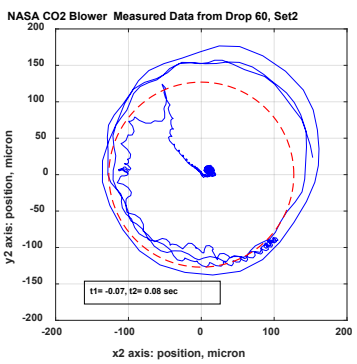

Figure 4a. Position sensor orbit (x2 vs y2) near initial drop contact at 60,000 rpm, vertical drop 60.

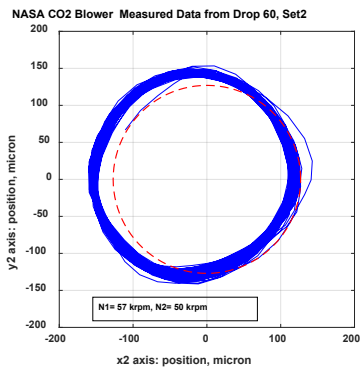

Figure 4b. Position sensor orbit (x2 vs y2) from 57 krpm to 50 krpm during spin down, vertical drop 60.

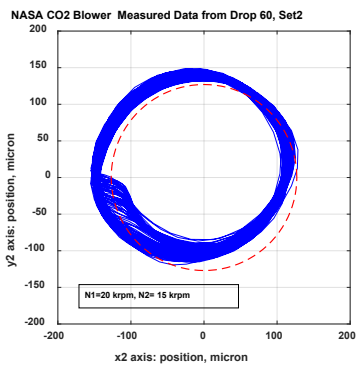

Figure 4c. Position sensor orbit (x2 vs y2) from 20 krpm to 15 krpm during spin down, vertical drop 60.

Figures 5 and 6 show color intensity waterfall plots of the entire spin down for horizontal drop 50 and vertical drop 60. In both plots, the highest intensity (highest amplitude) is the primary whirl orbit that starts at about 180 Hz and drops

in frequency as speed falls. In the horizontal case, Fig. 5, the whirl begins to die out as the spin speed falls below 200 Hz (12,000 rpm). In Fig. 6, the vertical case, the whirl persists to a lower speed as expected. There is also a smaller second harmonic representing the ovality of the whirl orbit.

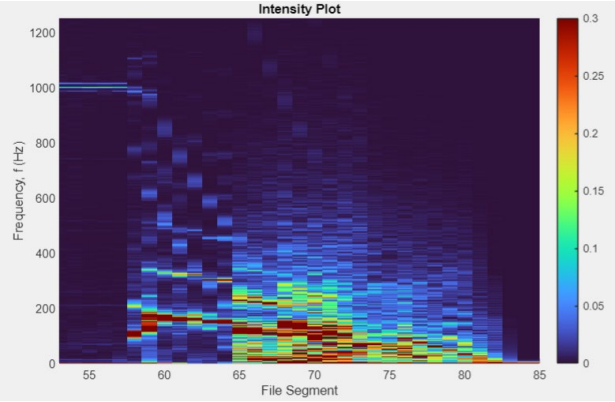

Figure 5. Position sensor x2, frequency spectrum vs. time, during spin down, horizontal drop 50.

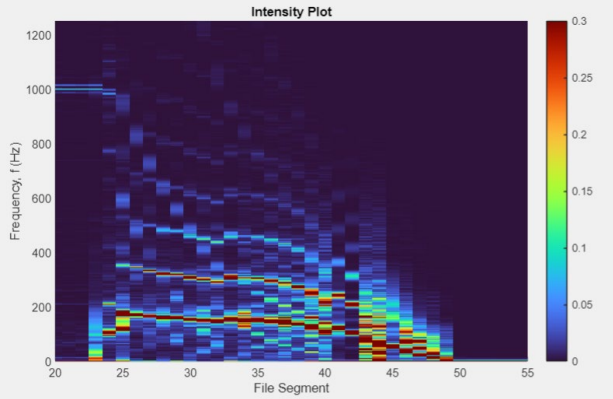

Figure 6. Position sensor x2, frequency spectrum vs. time, during spin down, vertical drop 60.

Figure 7-8 shows the primary whirl frequency vs. spin speed for selected drop/spin downs. Figure 7 is for horizontal drops and Fig. 8 is for vertical drops. For the horizontal drops, the primary whirl frequency starts at 170 to 178 Hz and then falls as speed decreases. This is primarily due to the decrease in aerodynamic axial load which decreases with the speed squared. The forward tangential force that drives forward whirl is proportional to the axial force reacted by the thrust backup bearing. A secondary reason is the O-ring stiffness drops as the whirl amplitude drops. For the vertical drops, the whirl frequency starts a bit higher at 165 to 188 Hz and falls with speed as with the horizontal drops. The forward whirl persists to lower spin speeds in the vertical cases due to a higher thrust load and lack of a fixed direction radial load. Recall from Fig. 4c that at lower speeds the whirl orbit does not execute a full circle around the bearing.

It is atypical to have so much variation in the primary whirl frequency. One explanation is the low squeeze (pre-strain) required for the O-ring mounts allows for more run-to-run variation in the whirl frequency. Since elastomer stiffness varies with temperature, a large variation in the steady pre-drop operating temperature might also explain the frequency variation. But a comparison of pre-drop temperatures to measured whirl frequencies did not uncover a correlation. Anders [7] observed that the forward whirl frequency tends to increase as the number of landings (drops) increase and the bearings approach failure. Although the authors have observed this on drop test programs, it was not clearly seen here, probably because the bearings are not particularly close to failure even after 100 drops and spin downs.

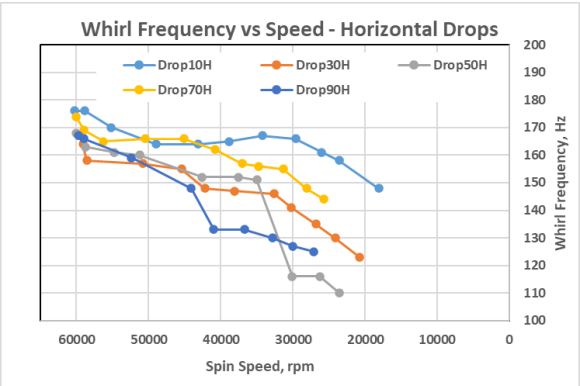

Figure 7. Primary whirl frequency vs. spin speed for horizontal rotor, bearing Set2.

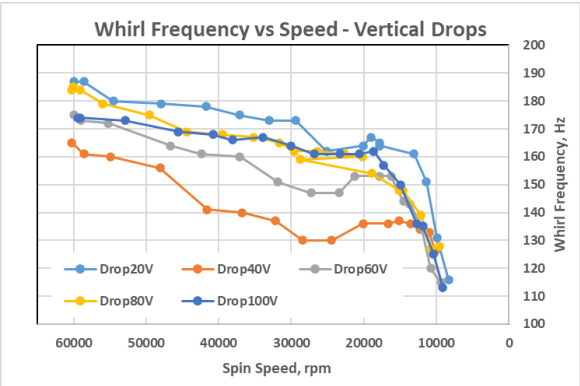

Figure 8. Primary whirl frequency vs. spin speed for vertical rotor, bearing Set2.

5.0 Inspection Results

All bearings from the two test series (Set1 and Set2) were disassembled and inspected by an outside vendor at the completion of testing. The bearings from Set2 were also disassembled and inspected after 60 drops (out of 100 drops).

Figure 9 is a picture of inlet, inboard backup bearing (from Set1) showing inner ring raceway and ball path after 30 drops. The inner ring raceway possesses light, false brinelling, silver plating worn from the ball path, and frosting with the ball path (arrow) high up on the raceway shoulder. The dimensional inspections of all four bearings found only minor raceway asperities likely due to movement of the silver plating on the bearing raceways. The basic curvatures and surface condition indicated no significant base metal wear or spall damage.

Figures 10a and 10b are pictures of the inlet, outboard backup bearing (from Set2) showing the inner ring raceway after 60 and 100 drops respectively. The outboard bearing carries the thrust load across the ball train into the housing. The raceway exhibits minor removal of the silver plating with fine debris dents. No spalling, brinelling, or misalignment is apparent. As with Set1, dimensional inspections of all four bearings found only minor raceway asperities from movement of the silver plating on the raceways. The curvatures and surface condition indicated no significant base metal wear or spall damage.

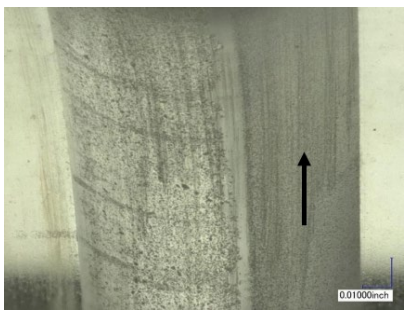

Fig. 9. Photo of inlet, inboard bearing (from Set1) showing inner ring raceway after 30 drops.

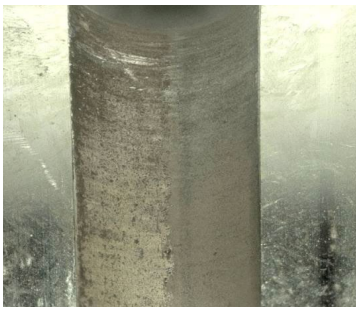

Fig. 10a. Photo of inlet, outboard bearing (from Set2) showing inner ring raceway after 60 drops.

Fig. 10b. Photo of inlet, outboard backup bearing (from Set2) showing inner ring raceway after 100 drops.

Figure 11 is a picture of the inlet, inboard backup bearing (from Set2) showing the bore after 100 drops. The bore surface shows light fretting and brownish deposits. The fretting is primarily due to the slipping that occurs just after drop down as the inner ring spins up to shaft speed and is considered normal. Figure 12 shows one of the ceramic balls from the Set2, inlet, inboard bearing. It is in good condition, exhibiting light black colored deposits, likely silver plating, with no apparent wear or surface damage. Overall, the bearings are still in good condition after 100 drops and spin downs.

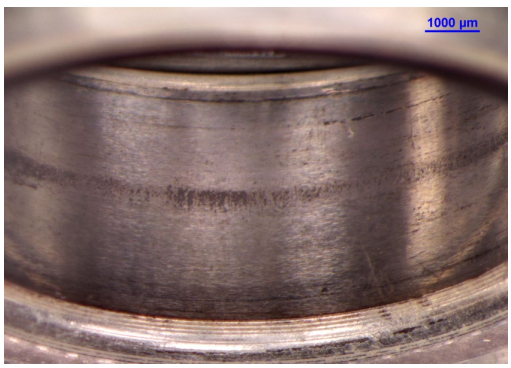

Fig. 11. Picture of inlet, inboard backup bearing (from Set2) showing bore after 100 drops.

Fig. 12. Showing a ceramic ball from the inlet, inboard backup bearing (from Set2) after 100 drops

6.0 Simulation Results

Nonlinear rotordynamic simulations were run during the design phase to evaluate resilient mount properties and backup bearing loading during a drop and spin down [1]. Updated simulations were run post drop testing to reassess bearing loads based on the test results with the primary change being updates to the modelling of the O-ring resilient

elements. In the simulation tool [8], the rotordynamic equations of motion of a coupled, flexible rotor/housing system (the blower) are numerically integrated using the Newmark-Beta method. The transient and/or nonlinear forces are updated at each integration step and added to the force vector. Magnetic bearing position loop and current loop outputs are updated at same rate as the MBC hardware. Modelling backup bearing clearance, amplitude dependent stiffness and damping, magnetic bearing saturation characteristics, and external housing forces are straightforward with this approach. The forces produced by rotor contact with the axial backup bearing are updated using the Wilkes method [4].

Simulation results are presented in Figs. 13-17. Figures 13-15 show predicted displacement at the inlet end sensor and are comparable to the measured results in Figs 3 and 4 for the same sensor location. The simulation shows a few rotor bounces on initial drop contact followed by a few backward whirl cycles as the backup bearing inner ring comes up to spin speed; the whirl direction then reverses to forward whirl and remains that way for the duration of the spin down. Note that in the simulation the spin direction is CCW (x to y) whereas in the blower the spin direction is CW (y to x). The predicted amplitudes of ~150um are similar to the measurement. There are 6 backward whirl cycles predicted compared to two in the measurement – this likely indicates the simulation overpredicts the time for the inner ring to reach full speed. The predicted whirl frequency from the simulation is 160 Hz, on the low side of the measurements shown in Fig. 6. Figure 16 shows relative displacement across the resilient mount as the rotor coasts from 57,000 rpm to 50,000 rpm. Figure 17 shows predicted loads from the drop and spin down. The contact stresses imposed by the peak loads at the drop transient (including 240 N peak axial) are moderate. The contact stresses during spin down are low for a backup bearing application.

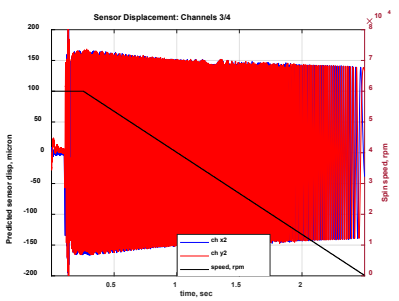

Fig. 13a. Predicted position vs. time for x2 and y2 sensors, during drop and spin down, vertical rotor, drop 60

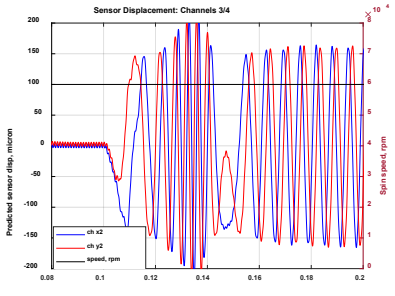

Figure 13b. Predicted position v time for x2 and y2 sensors, during initial portion of drop 60 with vertical rotor.

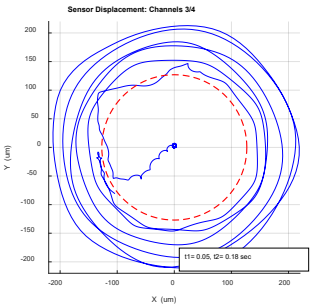

Figure 14. Predicted position sensor orbit (x2 vs y2) near initial drop contact at 60,000 rpm.

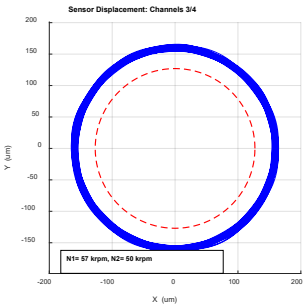

Fig. 15. Predicted position sensor orbit (x2 vs y2) from 57 krpm to 50 krpm during spin down.

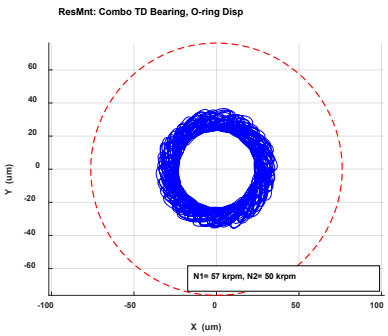

Fig. 16. Predicted relative disp across resilient mount (x2 vs y2), 57 krpm to 50 krpm during spin down.

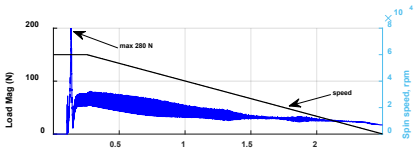

Fig. 17. Predicted backup bearing loads during spin down.

7.0 Conclusions

Two series of drop and spin down tests were conducted on an AMB supported blower used on the ISS. The first test series consisted of 30 drops and spin downs from 60,000 rpm on a new set of backup bearings (Set1). The second series consisted of 100 drops and spin downs from 60,000 rpm on a second set of backup bearings (Set2). Half of the tests were conducted with the rotor spin axis horizontal and the other half with the spin axis vertical. Both sets of bearings performed as designed.

1) The dynamic performance during drop and spin down, observed via the position sensors, was well behaved and followed expected trends.
2) Forward whirl frequency varies more than typical which is attributed to low pre-strain on the elastomeric O-ring mount.
    a. Vertical testing – whirl persisted to lower speeds than horizontal.
    b. Horizontal testing – whirl persisted longer than typical for horizontal machines. This is attributed to the characteristic that the aerodynamic load is much higher than the fixed direction radial load.
3) Post test inspection found the bearings to be in good condition with very little base metal wear. The Set2 bearings were judged to still have considerable usable life after 100 drops and spin downs.
    a. This outcome is due to the design characteristics of the blower which allowed a design with low speed factors, low loads, fast spin down and moderate temperatures.
4) A numerical simulation produced displacement and frequency predictions well aligned with the test results. Thus, bearing loads and contact stresses predicted from the simulation should be a good indicator of performance.

8.0 Acknowledgement

The work reported here was supported by NASA Contract 80JSC021D0009, Program Managers: John Garr and Chris Brown of the NASA ISS Vehicle Office, Houston, Tx.

References

[1] Hawkins, L., Filatov, A., Khatri, R., DellaCorte, C., Howard, A., 2020, "Design of a Compact Magnetically Levitated Blower for Space Applications", GTP-21-1084, *J. of Eng. For Gas Turbines and Power*, Vol. 143, pp. 091012, September.

[2] Hawkins, L., Khatri, R., Filatov, A., DellaCorte, C., Howard, A., 2021, "Random Vibration Simulation and Testing of a Compact, Magnetic Bearing Supported Blower for Space Applications," *Proc. 17th Int. Symp. Magnetic Bearings*, Paper 72, Rio de Janeiro, Brazil, Virtual

[3] Khatri, R., et.al, 2024, "Commissioning and Operational Data of Advanced Magnetic-Bearing-Supported Carbon Dioxide Blower for Space Applications," *53rd Int. Conf. on Environmental Sys*, ICES-2024-278, Louisville, KY.

[4] Wilkes J., Moore, J., Ransom, D. and Vannini, G., 2013, "An Improved Catcher Bearing Model and Explanation of the Forward Whirl/Whip Phenomenon Observed in Active Magnetic Bearing Transient Drop Experiments," *Proc. of ASME Turbo Expo*, GT2013-94594, San Antonio, TX, June.

[5] Bormann, A., Gasch, R., 2004, "Damping and Stiffness Coefficients of Elastomer Rings and Their Optimised Application in Rotor Dynamics," *Australian J. of Mechanical Engineering.*, Vol. 1, No. 2, pp. 91-101.

[6] Caprio, M., Murphy, B,, Herbst, J., 2004, "Spin Commissioning and Drop Tests f a 130 kW-hr Composite Flywheel," *Proc. 9th Int. Symp. Magnetic Bearings*, Paper 65, Lexington, KY.

[7] Anders, M.J., Leslie, M.P., Stacke, M.L., 2013, "Rotor Drop Simulations and Validation with Focus on Internal Contact Mechanisms of Hybrid Ball Bearings," *Proc. of ASME Turbo Expo*, GT2013-95816, San Antonio, TX, June.

[8] Hawkins, L., Wang, Z., Nambiar, K., 2018, "Floating Shock Platform Testing of a Magnetic Bearing Supported Chiller Compressor – Measurements and Simulation Results", *ASME Turbo Expo*, Paper GT2018-77031, June, Oslo, Norway.